Impairment of cyclo-oxygenase-2 function results in abnormal growth plate development and bone microarchitecture but does not affect longitudinal growth of the long bones in skeletally immature mice

Original Article

CARTILAGE
2021, Vol. 12(3) 387–398

DOI: 10.1177/1947603519833149
journals.sagepub.com/home/CAR

Impairment of Cyclo-oxygenase-2 Function Results in Abnormal Growth Plate Development and Bone Microarchitecture but Does Not Affect Longitudinal Growth of the Long Bones in Skeletally Immature Mice

Marjolein M. J. Caron[1], Tessy M. R. Castermans[1], Bert van Rietbergen[1,2], Mirella J. J. Haartmans[1], Lodewijk W. van Rhijn[1], Adhiambo M. A. Witlox[1*], and Tim J. M. Welting[1*]

Abstract

Objective. Despite the general awareness that cyclo-oxygenase-2 (COX-2) is crucial for endochondral ossification, the role of COX-2 in skeletal development is largely unknown. We hypothesized that inhibition or genetic loss of COX-2 leads to impaired growth plate development and consequently impaired postnatal development of the long bones. *Design*. Skeletally immature (5 weeks old) B6;129S-Ptgs2^{tm1Jed}/J wildtype mice were treated for 10 weeks with celecoxib (daily oral administration 10 mg/kg) or placebo and compared with B6;129S-Ptgs2^{tm1Jed}/J homozygous knockout mice ($n = 12$ per group). *Results*. Fifteen weeks postnatally, no significant difference in growth plate (zone) thickness was found between groups. However, significantly higher proteoglycan content and lower expression levels of collagen type II and X staining in the growth plates of celecoxib-treated mice, and to a lesser extent in COX-2 knockout mice. In addition, a significantly decreased cell number and cell size were observed in the hypertrophic zone of the growth plates of both experimental groups. Micro–computed tomography analysis of the subchondral bone region directly beneath the growth plate showed significantly higher bone density and trabecular thickness, following celecoxib treatment. Despite the detected differences in growth plate extracellular matrix composition and subchondral bone morphology, no difference was found in the length of the tibia in celecoxib-treated mice or COX-2 knockout mice. *Conclusions*. Genetic loss of COX-2 or treatment with celecoxib did not result in detectable differences in gross murine formation of the tibia or femur. However, there were notable phenotypic features detected in the maturation of the growth plate (hypertrophic zone and subchondral bone) as a result of the celecoxib treatment.

Keywords

celecoxib, COX-2, skeletal development, endochondral ossification, growth plate

Introduction

The development of the major part of the mammalian skeleton, as well as bone fracture healing, depends on a complex cellular process, which is defined as endochondral ossification.[1,2] During skeletal development, this process takes place in the growth plates, which are located in the epiphyseal regions of developing long bones. The developing growth plate is a unique cellular phenomenon with a high degree of organization. Histologically, the growth plate can be divided into four different zones: resting zone, proliferative zone, hypertrophic zone, and mineralization/ossification zone. Functionally, these zones

[1]Department of Orthopedic Surgery, CAPHRI Care and Public Health Research Institute, Maastricht University Medical Center, Maastricht, the Netherlands
[2]Orthopaedic Biomechanics, Department of Biomedical Engineering, Eindhoven University of Technology, Eindhoven, the Netherlands

*Adhiambo M. A. Witlox and Tim J. M. Welting contributed equally to the study.

Corresponding Author:
Marjolein M. J. Caron, Department of Orthopedic Surgery, CAPHRI Care and Public Health Research Institute, Maastricht University Medical Center. P.O. Box 5800, 6202 AZ, Maastricht, the Netherlands.
Email: marjolein.caron@maastrichtuniversity.nl

represent different dedicated cellular compartments in which cells with progenitor activity in the resting zone differentiate into proliferating chondrocytes, which finally transdifferentiate into osteoblasts[3-5] or die by apoptosis as a result of hypertrophic differentiation. This latter event generates a collagenous and premineralized scaffold that is populated and ossified by osteoblasts and remodeled by osteoclasts to form new bone. In analogy to the growth plate, endochondral ossification also drives most of the bone fracture repairs by ossification of the initial cartilaginous fracture callus tissue. The resulting mineralized tissue is subsequently ossified by osteoblasts and remodeled by osteoclasts to restore the original architecture of the fractured bone.

Growth plate activity is directly responsible for skeletal growth and its *de novo* bone-generating activity peaks during *in utero* development of the fetus, the first months after birth, and during puberty.[6] During these phases of development, the growth plates are most vulnerable to disturbances that may lead to abnormal skeletal development, presenting as malformations, dwarfisms, gigantisms, and others.[6,7] These disturbances of growth plate development can originate from genetic factors (>200 different types of skeletal conditions have a known genetic origin[8,9]), trauma, and nutritional factors.[10,11]

Selective cyclo-oxygenase-2 (COX-2) nonsteroidal anti-inflammatory drugs (NSAIDs) are widely used analgesics but have been reported to impair endochondral ossification-driven fracture healing by interference with the ossification phase and inhibiting osteoblast activity.[12-14] Similarly, COX-2 knockout mice show impaired fracture healing, which is also attributed to impaired osteogenesis.[15] However, our recent work showed that the COX-2 selective NSAID celecoxib also affects endochondral ossification at the chondrocyte level by impairing the level of chondrocyte hypertrophy, even in the developing growth plate.[16] In addition, we found that during chondrogenic differentiation *in vitro* COX-2 expression correlates with expression of chondrocyte hypertrophic markers and that COX-2 is mainly expressed in the hypertrophic zone of the growth plate.[16] Together this introduces a whole new view on the action of COX-2 during the chondrogenic phase of endochondral ossification.

Despite the general awareness that COX-2 specific NSAIDs affect endochondral ossification, the involvement of COX-2 in skeletal development has not been investigated yet. Therefore, we hypothesized that inhibition of COX-2 enzymatic activity by celecoxib or genetic loss of COX-2 leads to alterations in growth plate development with consequences for postnatal longitudinal growth of the long bones. To test this hypothesis, we measured the growth plate thickness and extracellular matrix composition as well as the morphology of the newly formed bone postnatal in the tibia and femur of COX-2 knockout, wildtype, and wildtype celecoxib-treated mice.

Materials and Methods

Experimental Design and Animal Model

For this study 24 healthy skeletally immature (5 weeks old, ±20 g) B6;129S-Ptgs2$^{tm1Jed/J}$ wildtype mice and 12 B6;129S-Ptgs2$^{tm1Jed/J}$ homozygous knockout mice were used (Jackson Laboratories, Bar Harbor, ME, USA).[17] Genotyping was performed with DNA from toe biopsies using the following primers: 5′-GCCCTGAATGAACTGCAGGACG-3′, 5′-CAC GGGTAGCCAACG-CTATGTC-3′, 5′-CACCATAGAAT CCAGTCCGG-3′, and 5′-ACCTCTGCGATGCTCTTCC -3′. The experiment was approved by the Maastricht University animal ethical committee (MUMC DEC approval 2013-094) and we confirm that all experiments were performed in accordance with relevant guidelines and regulations (ARRIVE, Animal Research: Reporting of In Vivo Experiments). Sample size was calculated according to the formula of L. Sachs ($\alpha = 0.05$, power = 80%) $n =$ (expected standard deviation: 0.20/expected effect size: 0.25)2 * 15.7), corrected for potential dropout, and 12 animals per group were included (6 female and 6 male mice). Throughout the experiment, animals were housed in groups under standard conditions with *ad libitum* access to water and food and 12 hours of light each day. Animal well-being and weight was monitored daily. Wildtype animals were randomly assigned to the treatment or control group (50% male/female ratio was maintained). Celecoxib (10 mg/kg) (Pfizer) or placebo (water) was orally administered to B6;129S-Ptgs2$^{tm1Jed/J}$ wildtype mice from the first day of the experiment (day 0) on a daily basis by oral gavage. B6;129S-Ptgs2$^{tm1Jed/J}$ homozygous knockout mice also received placebo treatment. After 10 weeks mice were euthanized by O_2/CO_2 asphyxiation. During further processing, the specimens were coded and the researchers thus blinded to the treatment received. One B6;129S-Ptgs2$^{tm1Jed/J}$ homozygous knockout mouse died during the experiment due to complications after oral gavage.

Prostaglandin E_2 Measurement

To confirm COX-2 inhibition by celecoxib we determined prostaglandin E_2 (PGE_2) levels in blood plasma at sacrifice by standardized enzyme immunoassay (EIA) analysis. Briefly, blood was drawn from the animals and centrifuged at 1300 rpm for 5 minutes. The blood plasma was used to perform a standardized EIA for detection of PGE_2 levels according to the manufacturer's protocol (Cayman Chemicals, Ann Arbor, MI, USA).

Determination of Growth Plate Morphology by (Immuno)Histochemistry

Whole knee joints were isolated for histology, fixed in phosphate buffered formalin for 7 days followed by decalcification in 0.5 M ethylenediaminetetraacetic acid (EDTA) pH 7.8 for 3 weeks and subsequently embedded in paraffin using standard procedures. Coronal tissue sections of 5 μm were prepared. Before histochemistry, tissue sections on slides were deparaffinized and rehydrated using standard protocols. Sections for growth plate and cell surface measurements were stained with hematoxylin (Dako). Proteoglycans were stained with Safranin-O (0.05%) and counterstained with Fast Green (0.1%). For determination of cell number, sections were stained with DAPI (4′,6-diamidino-2-fenylindool; Thermo Fisher). For the analysis of osteoclastic activity, Tartrate-resistant acid phosphatase (TRAP) staining (pH 4.7-5.0 at 37°C) combined with Fast Green (0.02%) counterstaining and Methyl Green (0.5%; pH 4.2) nucleus staining was used to visualize TRAP-positive (TRAP+), nucleus-containing cells. Stained sections were dehydrated and mounted in Histomount (Thermo Shandon) for microscopic analysis. Specialized software was used to quantify Safranin-O intensity (ImageJ), cell number and cell size (CellProfiler). All nucleus containing TRAP+ cells were manually counted in the region beneath the growth plate.

For immunohistochemical analysis of collagen type II (Col2a1) and collagen type X (Col10a1) in growth plate sections, rehydrated sections were treated with 0.4% hyaluronidase. Endogenous peroxidase activity was inactivated by peroxidase-blocking solution (Dako, REAL) and samples were blocked with 10% normal goat serum for 30 minutes. Mouse monoclonal anti-Col2a1 (II-II6B3; Developmental Studies Hybridoma Bank) and mouse negative control IgG1 (negative control; Dako) were used at 1:100 and same IgG1 concentration, respectively. Rabbit polyclonal anti-Col10a1 (Quartett) and negative control nonimmune normal rabbit serum (negative control) were used at 1:100. Unbound antibodies were removed by washing with phosphate buffered saline containing 0.1% Tween-20. Bound antibodies were visualized with horse radish peroxidase (HRP) labelled anti-rabbit or anti-mouse secondary antibodies (Dako, EnVision+ System-HRP labeled polymer) by incubation for 30 minutes at room temperature. Unbound antibodies were removed by rinsing in PBS-T (phosphate buffered saline with Tween-20). For detection, DAB (3,3′-diaminobenzidine) chromogen substrate (Dako) was used. Stained sections were mounted in Histomount as described above.

Bone Length Measurements

After dissection of the hind limb, length of femur and tibia was measured using a digital micrometer, and these knee joints were subsequently processed for histology. Hematoxylin-stained sections from similar middle regions of the growth plate of each mouse were analyzed using a Zeiss Axioscope A.1 (with AxioVision 4.8 software). The anatomical middle of the growth plate was determined in the sections by measuring the total width (from medial to lateral) of the growth plate and the middle was set at half of this value. Furthermore, we confirmed that this middle point corresponded with anatomical features of the joint such as the intercondylar eminence of the tibia and the patellofemoral groove in the femur. The anatomical middle of the growth plates of femur and tibia was used as an internal reference point. From each growth plate 3 consecutive sections were measured at the middle, a quarter and half the distance from the anatomical reference point for determination of the thickness of the total growth plate, the resting, proliferative, and hypertrophic zones.

Determination of Bone Morphology by Micro–Computed Tomography

After dissection of the hind leg, the growth plate region of the tibia of each sample was scanned in a micro–computed tomography scanner (μCT 80, Scanco Medical AG, Wangen-Brüttisellen, Switzerland) at a resolution of 10 μm (voltage 55 kVp; intensity 145 μA; integration time 200 ms) in the air in a closed holder. Micro-CT image processing included Gauss filtering (sigma = 0.4, support = 1 voxel) and segmentation of the bone phase using a global threshold of 210 per mile of the maximum gray value, corresponding to 453 mg hydroxyapatite (HA)/cm^3.

Contours were drawn manually to identify a volume of interest (VOI) of subchondral bone just distal of the growth plate with a thickness of approximately 200 μm (VOI-1, **Fig. 3A**). Following this, the region identified by the contours was shifted in the distal direction by 200 μm (VOI-2, **Fig. 3A**), which thus encompasses the bone further away from the growth plate. For analysis of the growth plate region itself, the contour was shifted in the proximal direction by 100 microns, which was the typical thickness of the growth plate region as seen on the micro-CT scans. Only the region that was nonoverlapping with the original contoured region was then analyzed (VOI-3).

From the segmented images, the following morphology indices were determined for the indicated VOI's: tissue bone mineral density, bone volume fraction (BV/TV), trabecular number (Tb.N), trabecular thickness (Tb.Th), and trabecular separation (Tb.Sp).[18,19]

Determination of Bone Turnover by Alkaline Phosphatase Activity

Enzymatic activity of alkaline phosphatase (ALP) was determined in cortical bone samples using a colorimetric assay. Tissue was pulverized using a micro-dismembrator

(Braun Biotech; 300 rpm for 1 minute) and dissolved in freshly prepared collection buffer (1.5 M Tris-HCl pH 9.0; 2% v/v Triton X-100). In flat-bottom 96-well plates, containing assay buffer (1.5 M Tris-HCl pH 9.0; 1 mM ZnCl2; 1mM MgCl2; 7.5 mM *p*-nitrophenyl phosphate), ALP activity was determined by measuring the ALP-depend enzymatic conversion of *p*-nitrophenyl phosphate to nitrophenyl phosphate by spectrophotometric analyses at 405 nm. A calibration curve containing an increasing concentration of nitrophenyl phosphate was used to determine the absolute amount of ALP-generated nitrophenyl phosphate in time. Values were normalized to total DNA concentration and expressed as units ALP activity (1U = 1 fmol nitrophenyl phosphate/min/mg).

Hydroxyproline Assay

Hydroxyproline levels are determined in cortical bone samples by the reaction of oxidized hydroxyproline with 4-(dimethylamino)benzaldehyde (DMAB), which results in a colorimetric (560 nm) product, proportional to the hydroxyproline present.[20] A serially diluted standard curve of hydroxyproline (Sigma-Aldrich) in HCl (12 M) was included to quantify the hydroxyproline concentration in the samples. Before measurement, samples in ALP collection buffer (see above) were diluted in HCl and standards were prepared and heated to 120°C for 10 minutes after which citric acid solution (1.4 M) was added. Samples were oxidized using chloramine-T solution (Sigma-Aldrich) and mixed with DMAB/perchloric acid solution at 65°C followed by spectrophotometric analyses at 560 nm. Hydroxyproline concentration was determined using the standard curve and normalized to total DNA concentration.

DNA Quantification

DNA concentration in samples used for ALP and hydroxyproline assay was determined using SYBR Green I Nucleic Acid stain (Invitrogen). A serially diluted standard curve of genomic control DNA (calf thymus, Invitrogen) in TE buffer (10 mM Tris/HCl pH 8.0, 1 mM EDTA) was included to quantify the DNA concentration in the samples. Before measurement, samples were diluted in TE buffer (1 µL sample and 99 µL TE buffer) and standards were prepared. SYBR Green was diluted 10,000 times in TE buffer and 100 µL of this solution was added to 100 µL of the above-prepared samples or standards. Fluorescence was determined in standard 96-well ELISA (enzyme-linked immunosorbent assay) plates in a Spectramax M2 microplate reader (Molecular Devices): excitation 488 nm and emission 522 nm. DNA concentration was determined using the standard curve.

Statistics

Statistical significance ($P < 0.05$) was determined by 1-way analysis of variance with Bonferroni correction using GraphPad Prism 5.0 (La Jolla, CA, USA). To test for normal distribution of the input data, D'Agostino-Pearson omnibus normality tests were performed. Equality of variance was tested by Bartlett's test for equal variances. All quantitative data sets presented here passed the normality and variance tests. Lines in graphs represent the mean ± standard error of the mean (SEM).

Results

To determine if COX-2 inhibition by celecoxib or genetic loss of COX-2 leads to alterations in mammalian growth plate development with consequences for postnatal longitudinal growth of the long bones, we orally administered celecoxib (10 mg/kg/d; $n = 12$) or placebo (water; $n = 12$) to 5-week-old immature B6;129S-Ptgs2$^{tm1Jed/J}$ wildtype (WT) mice, or placebo-treated 5-week-old immature B6;129S-Ptgs2$^{tm1Jed/J}$ homozygous knockout (KO) mice ($n = 11$).[17] Genotype was confirmed by polymerase chain reaction. After 10 weeks, several growth plate and skeletal development parameters were determined.

COX-2 Inhibition by Celecoxib Does Not Alter Thickness of the Total Growth Plate or Different Growth Plate Compartments

PGE_2 measurement in blood plasma confirmed that celecoxib efficiently inhibited *in vivo* PGE_2 synthesis and thus systemically inhibited COX-2 enzyme activity (**Fig. 1A**). Interestingly, no significant differences in plasma PGE_2 levels were detected in COX-2 KO mice versus WT mice despite reduced COX-2 expression (Supplemental Fig. 1). No differences between groups were found in total weight at baseline or at sacrifice (**Fig. 1B**). To determine growth plate characteristics, growth plate sections of the proximal tibia were stained with hematoxylin. Analysis of the total growth plate thickness revealed no significant differences between groups, with a mean ± SEM thickness of 125.8 ± 3.86 µm in placebo-treated mice, 129.7 ± 5.75 µm in celecoxib-treated mice and 120.3 ± 2.20 µm in COX-2 KO mice (**Fig. 1C**). Growth plates were analyzed in more detail with regard to the different phases of growth plate chondrogenic differentiation; the thickness of the resting zone, proliferative zone, and hypertrophic zone was measured separately. The thickness of the resting zone (24.52 ± 2.04 vs. 28.33 ± 2.11 vs. 23.20 ± 1.28 µm), proliferative zone (60.12 ± 1.68 vs. 58.19 ± 2.83 µm) as well as the hypertrophic zone (39.75 ± 2.01 vs. 42.52 ± 2.61 vs. 38.82 ± 1.31 µm) of the placebo-treated versus celecoxib-treated versus COX-2 KO group,

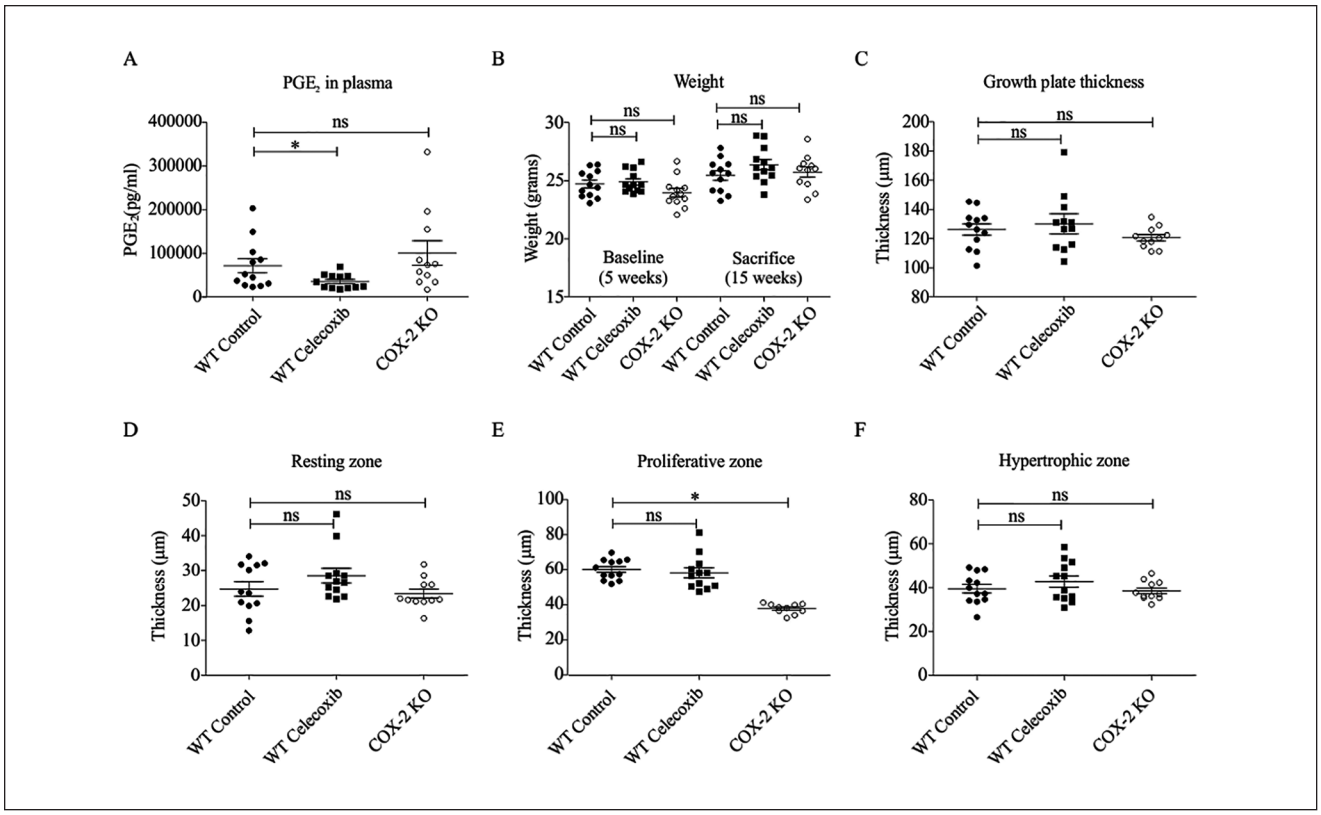

Figure 1. Growth plate measurements in wildtype (WT) control, cyclo-oxygenase-2 (COX-2) knockout (KO), and WT celecoxib-treated mice. Five-week old wildtype B6;129S-Ptgs2tm1Jed/J mice were treated with either celecoxib (10 mg/kg/d; $n = 12$) or placebo ($n = 12$) for 10 weeks and compared with B6;129S-Ptgs2tm1Jed/J homozygous knockout mice (placebo-treated; $n = 11$). At 15 weeks of age, prostaglandin E_2 (PGE_2), weight, and growth plate thickness of the proximal tibia was analyzed. (**A**) PGE_2 plasma levels. (**B**) The weight of the mice at baseline and at sacrifice. (**C**) The thickness of the growth plate was measured on hematoxylin-stained sections. (**D**) The thickness of the resting zone. (**E**) The thickness of the proliferative zone. (**F**) The thickness of the hypertrophic zone. Each dot represents the determined value for each of the individual mice and lines in graphs indicate mean ± standard error of the mean (SEM). Statistical significance: $^*P < 0.05$, *ns* = not significant.

respectively, did not differ significantly (**Fig. 1D-F**). Only the thickness of the proliferative zone in the COX-2 KO mice versus COX-2 WT mice was significantly decreased (60.12 ± 1.68 vs. 37.79 ± 0.92 μm). No significant results were found for measurements in growth plate sections of the distal femur (Supplemental Fig. 2). Together, this data shows that celecoxib-mediated COX-2 inhibition or genetic loss of COX-2 does not significantly affect the thickness of the different growth plate compartments in mice.

Celecoxib Alters Growth Plate Extracellular Matrix Composition and Number and Size of Hypertrophic Chondrocytes

Growth plate sections were studied in more qualitative detail. Safranin O staining revealed a macroscopically discernible higher proteoglycan content in the growth plates of celecoxib-treated mice compared to placebo-treated mice (**Fig. 2A**). Quantification of the intensity of Safranin O staining revealed a quantitatively higher ($P < 0.01$) Safranin O staining intensity in the proximal tibial growth plate of celecoxib-treated mice compared with placebo-treated mice (**Fig. 2B**). This difference was not observed in the COX-2 knockout mice. Significantly increased Safranin O staining intensity was found in the growth plate of the distal femur of both the celecoxib-treated mice and COX-2 knockout mice compared with placebo-treated mice (Supplemental Fig. 3).

Further analyses of the expression of extracellular matrix (ECM) protein type II collagen revealed a decreased expression of type II collagen in the growth plates of celecoxib-treated and COX-2 knockout mice, suggesting an altered ECM composition in the growth plates of these mice (**Fig. 2C**). Expression of type X collagen, a marker for a hypertrophic ECM, was very low (almost undetectable) in the celecoxib-treated mice compared with placebo-treated mice (**Fig. 2D**). The COX-2 KO group also presented with lower type X collagen expression. In contrast with a lack of

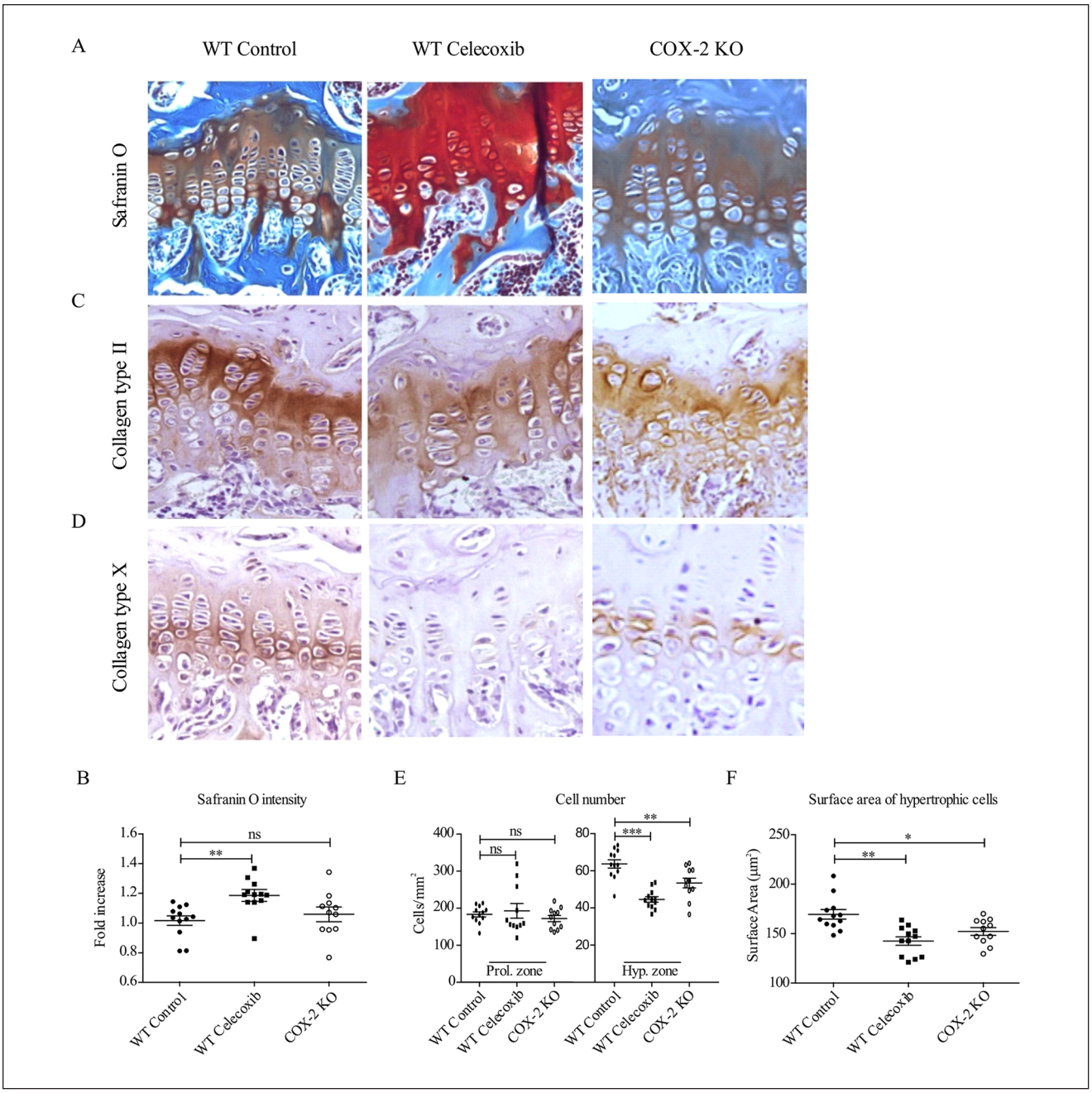

Figure 2. Growth plate stainings in control, celecoxib-treated mice, and cyclo-oxygenase-2 (COX-2) knockout (KO) mice. In adjacent growth plate sections of the proximal tibia from **Figure 1**; (immuno)histochemical stainings were performed and analyzed. (**A**) Safranin O/Fast Green staining. (B) Quantification of Safranin O staining intensity relative to wildtype (WT) control condition. (**C**) Collagen type II immunohistochemical staining. (**D**) Collagen type X immunohistochemical staining. (**E**) Cell number was determined in the proliferative and hypertrophic zone of the growth plate. (**F**) Surface area of the cells in the hypertrophic zone of the growth plate. Each dot represents the determined value for each of the individual mice and lines in graphs indicate mean ± standard error of the mean (SEM). Statistical significance: $*P < 0.05$, $**P < 0.01$, $***P < 0.0001$, ns = not significant.

significant difference in hypertrophic zone thickness (**Fig. 1F**), we found a significantly lower number ($P < 0.001$) of cells per surface area in the hypertrophic zone of growth plates from celecoxib-treated mice as well in COX-2 KO mice (63.41 ± 2.26 vs. 44.35 ± 1.47 vs. 53.18 ± 2.60 cells /mm^2), whereas no significant difference in cell number per surface area was observed in the proliferative zone of same animals (182.0 ± 6.76 vs. 191.4 ± 19.63 vs. 170.8 ± 8.44

cells/mm^2) (**Fig. 2E**). Interestingly, the cells present in the hypertrophic zone of the growth plates of celecoxib-treated mice and COX-2 KO mice were significantly ($P < 0.01$) smaller than in the placebo-treated mice (142.0 ± 4.23 vs. 151.6 ± 3.87 vs. 165.1 ± 5.86 μm^2) (**Fig. 2F**). Taken together, although no significant differences were observed in growth plate thickness or thickness of different growth plate compartments, the ECM composition, hypertrophic chondrocyte number and size in the growth plates of celecoxib-treated mice were markedly changed. For the COX-2 KO mice, only a reduced thickness of the proliferative zone was measured when compared with wildtype control mice, which was accompanied by a reduced collagen type II and X staining (but not Safranin O staining) and decreased hypertrophic cell number and size in the growth plates of these mice.

Bone Characteristics in Celecoxib-Treated Mice Compared with Placebo-Treated Mice

To determine if this aberrant growth plate phenotype due to COX-2 impairment resulted in a phenotype beyond growth plate (compartment) thickness, subchondral bone micro-CT characteristics directly beneath the growth plate were determined as a measure for bone (micro) structure as a direct result of bone remodeling during endochondral ossification. Because the celecoxib-treated mice showed the most aberrant growth plate phenotype, while the COX-2 KO mice showed an intermediate phenotype, we decided to compare the celecoxib-treated mice with the placebo-treated mice only. Micro-CT analysis of the subchondral bone region directly under the proximal tibia growth plate (VOI-1; **Fig. 3A**) showed significantly ($P < 0.05$) higher tissue bone mineral density (798.8 ± 4.15 vs. 812.2 ± 4.83 mg HA/cm^3), higher bone volume fraction (0.3382 ± 0.02 vs. 0.3954 ± 0.02), increased trabecular thickness (0.032 ± 0.00 vs. 0.035 ± 0.00 mm), and lower structure model index (data not shown), as a result of celecoxib treatment (**Fig. 3B** and **C**). No significant differences were found for number of trabecula (18.91 ± 0.48 vs. 19.20 ± 0.58 mm^{-1}), trabecular spacing (0.051 ± 0.00 vs. 0.048 ± 0.00 mm), and connectivity density (data not shown) (**Fig. 3C**). In the more distal region (VOI-2; **Fig. 3A**), the celecoxib-treated mice had an increased bone volume fraction and tissue bone mineral density compared with placebo-treated mice in this bone region as well (BV/TV: 0.3070 ± 0.02 vs. 0.2572 ± 0.01; bone density: 881.5 ± 7.82 vs. 852.8 ± 8.72 mg HA/cm^3) (**Fig. 3D**).

To establish if this different subchondral bone structure in the celecoxib-treated mice is altered due to changes in active bone remodeling, TRAP+ cells were counted in the VOI area as a measure of osteoclastic activity. Celecoxib treatment did not result in a significant difference in numbers of TRAP-positive cells compared with control mice (5557 ± 793.1 vs. 6732 ± 912.2 cells/cm^2) (**Fig. 3E**).

Finally, the total length of the tibia was measured and revealed no significant difference in the length in celecoxib-treated mice compared with placebo-treated mice (**Fig. 4A**; 17.88 ± 0.15 vs. 17.89 ± 0.10 mm). Also, COX-2 KO mice did not show a significant difference in length of the tibia (17.73 ± 0.19 mm). Similar results were found for femur (Supplemental Fig. 4). To get an indication of general bone quality, ALP activity and hydroxyproline content in cortical bone were measured. No significant difference was found in ALP activity or hydroxyproline content in the celecoxib-treated mice or COX-2 KO mice, compared with control mice (**Fig. 4B** and **C**).

In summary, there are no measurable differences found in the murine proximal tibia or distal femur formation as a consequence of COX-2 inhibition, while notable phenotypic features were found in the maturation of the growth plate (hypertrophic zone and subchondral bone) as a result from the absence of COX-2 activity, of which potential consequences are not yet understood.

Discussion

Endochondral ossification in the growth plate is directly responsible for pre- and postnatal skeletal growth. The selective COX-2 inhibitor celecoxib is a widely used analgesic but has been reported to impair endochondral ossification-driven fracture healing. Despite the general awareness that COX-2 affects endochondral ossification, a role for COX-2 in skeletal development is not described. We here show that there are no gross measurable differences in longitudinal growth of the murine proximal tibia or distal femur as a result of the genetic loss of COX-2 or treatment with COX-2 inhibitor celecoxib. However, we found notable phenotypic features in the postnatal development of the growth plates of tibia and femur as a result of celecoxib treatment.

Overall, we observed the most pronounced differences in postnatal growth plate characteristics in the control versus celecoxib-treated animals, whereas the growth plates of COX-2 KO mice seem to display a more intermediate phenotype, indicating differences in phenotypic penetrance when COX-2 is genetically lost or pharmacologically inhibited. Indeed, in **Figure 1A** we found that PGE_2 levels are significantly decreased in the celecoxib-treated mice, but not in the COX-2 KO mice. This is indicative of potential redundancy by COX-1 in PGE_2 synthesis in these mice. Gene expression analysis indeed revealed that decreased COX-2 expression was accompanied by increased COX-1 expression in the COX-2 KO mice compared with the WT mice (Supplemental Fig. 1). Whether the differences in growth plate characteristics can be attributed to deregulated downstream PGE_2 activity or activities of other COX-2-dependent prostanoids, and whether COX-1 plays a redundant role in this, remains to be elucidated.[21] In our earlier work,[16] we reported that

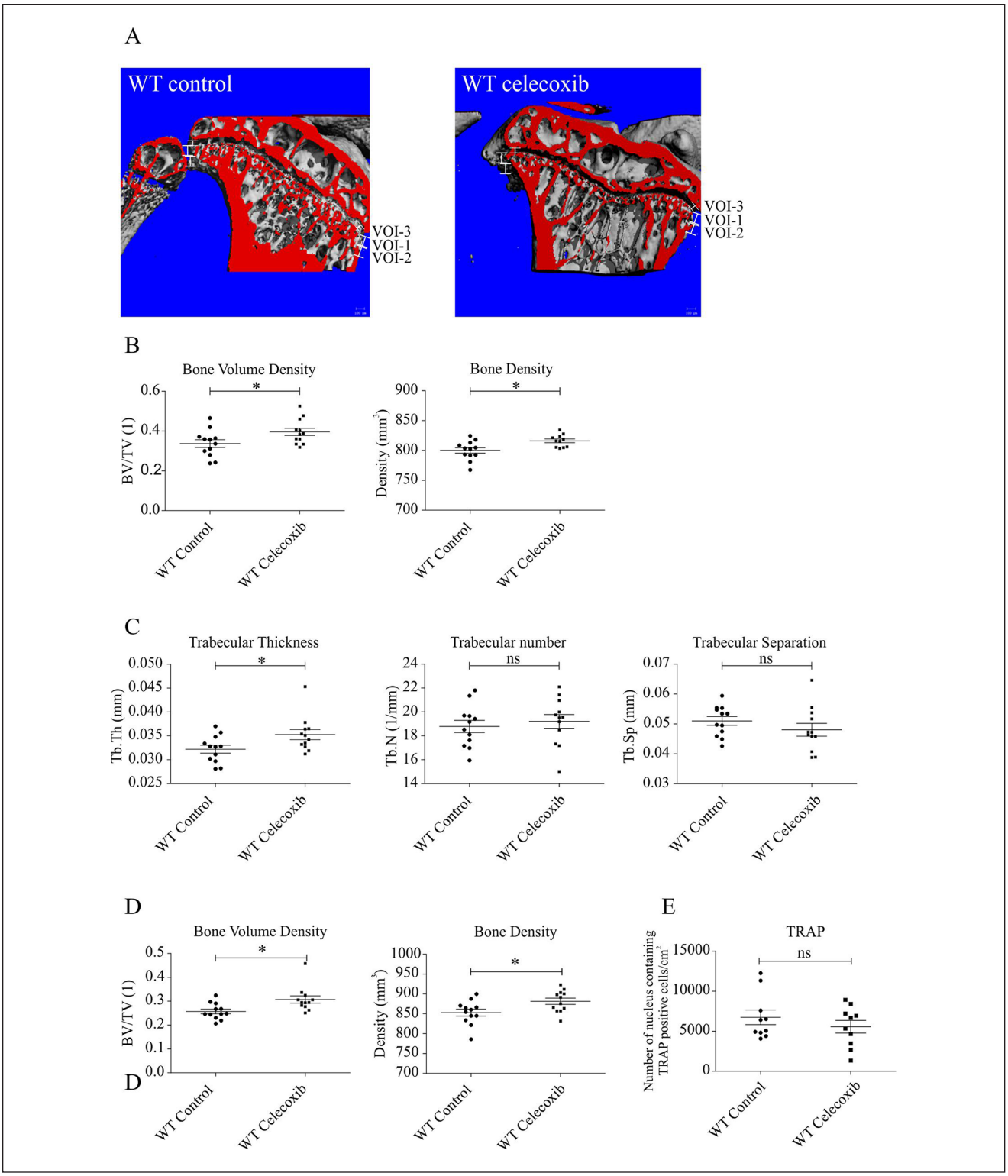

Figure 3. Bone microstructure analysis in control and celecoxib-treated mice. The bone microstructure was determined by micro–computed tomography (μCT). (**A**) Representative example of transections of a μCT image from control and celecoxib-treated mice. The volume of interest (VOI-1), VOI-2, and VOI-3 are indicated. (**B**) Quantification of bone volume density and bone density in VOI-1. (**C**) Quantification of trabecular thickness, number, and separation in VOI-1. (**D**) Quantification of bone volume density and bone density in VOI-2. (**E**) Nucleus containing tartrate-resistant acid phosphatase (TRAP)–positive cells were counted in 0.015 cm^2 region below the hypertrophic zone of the growth plate. Each dot represents the determined value for each of the individual mice and lines in graphs indicate mean ± standard error of the mean (SEM). Statistical significance: *$P < 0.05$, ns = not significant.

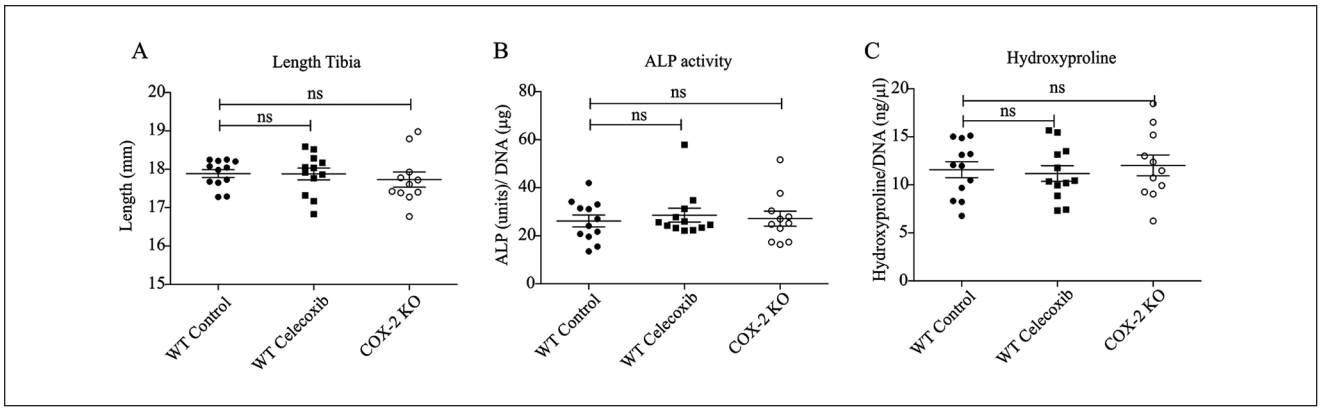

Figure 4. Length measurements of tibia in control, celecoxib treated mice and cyclo-0xygenase-2 (COX-2) knockout (ko) mice. Skeletal consequences of genetic loss of COX-2 or pharmacological inhibition by celecoxib was determined. (**A**) Length of the tibia was measured. (B) Alkaline phosphatase (ALP) enzymatic activity of cortical bone samples was determined and normalized to total DNA content. (**C**) Hydroxyproline levels corrected for DNA content were determined in cortical bone samples. Each dot represents the determined value for each of the individual mice and lines in graphs indicate mean ± standard error of the mean. Statistical significance: $*P < 0.05$, ns = not significant.

celecoxib-treatment of skeletally immature rabbits resulted in a decrease in the thickness of the hypertrophic zone of the postnatal growth plate. In the present study, we could not detect significant differences in the thickness of the hypertrophic zone in the COX-2 KO and celecoxib-treated mice. However, and in concert with our previous findings,[16,22] we did detect local changes in the hypertrophic zone, including lower levels of collagen type X expression in these mice. When COX-2 KO mice were analyzed at an earlier developmental stadium (5 weeks postnatally) we did find more pronounced effects (in a similar direction as at 15 weeks of age) especially for the tibia, regarding total growth plate thickness and thickness of the hypertrophic zone when compared with WT control littermates (Supplemental Fig. 5). Overall this indicates a clear relationship between the expression of collagen type X, chondrocyte hypertrophy and COX-2 enzyme activity. Indeed, COX-2 and collagen type X are both expressed in the hypertrophic zone of the growth plate and Gu *et al*.[23] found a molecular interaction between COX-2 and a Col10a1 *cis*-enhancer, supporting a role for COX-2 as a candidate Col10a1 regulator.[16,21] Alternatively, the observed effects may be a result of a deregulated COX-2/PGE_2/BMP-2 signaling axis. Chondrocyte hypertrophy and thus collagen type X expression, are, at least in part, regulated by BMP-2-induced Smad1/5/8 signaling, and this signaling axis is sensitive to PGE_2 regulation.[16,24-28] Decreased COX-2 function, either by genetic loss or pharmacological inhibition, might therefore directly or indirectly affect chondrocyte hypertrophic differentiation and the smaller cell size of the growth plate hypertrophic chondrocytes strongly indicates that on COX-2 inhibition, cells are indeed hampered in their differentiation process in becoming fully differentiated hypertrophic chondrocytes.[29,30] Interestingly, the majority of our significant findings between WT mice and celecoxib treated WT mice or COX-2 KO mice in the growth plate are found in the hypertrophic zone and subchondral bone. This is exactly the region were vascular channel development takes place; a process essential for remodeling of the hypertrophic zone to bone tissue during endochondral ossification and which is under tight control of vascular endothelial growth factor (VEGF).[31-34] Furthermore, COX-2 expression is found in the hypertrophic zone of the growth plate[16,21] and can be induced by hypoxia-stimulated VEGF secretion[35] and vice versa; VEGF expression can be increased by COX-2 signaling via the protein kinase C pathway.[36] It might therefore be possible that COX-2 inhibition results in abnormal VEGF expression and vascularization of the hypertrophic zone of the growth plate and subchondral bone leading to disrupted growth plate remodeling that is seen in this study. Further research is needed to address the role of VEGF and vascular channel development in the COX-2 KO or celecoxib-treated mice. Another important feature of hypertrophic differentiation in the growth plate is apoptosis; hypertrophic cells die and leave their extracellular matrix behind for osteoblasts to adhere and remodel into bone.[1,2] In cancer treatment, COX-2 inhibition is described to increase apoptosis by several potential mechanisms, including increased expression of death signals like ceramide and downregulating the anti-apoptotic proteins Bcl-2 and Akt.[37] Although little is known about the relation of COX-2 inhibition and apoptosis in growth plate development,[38,39] increased apoptosis may offer an explanation for the observed decrease in cell number seen in

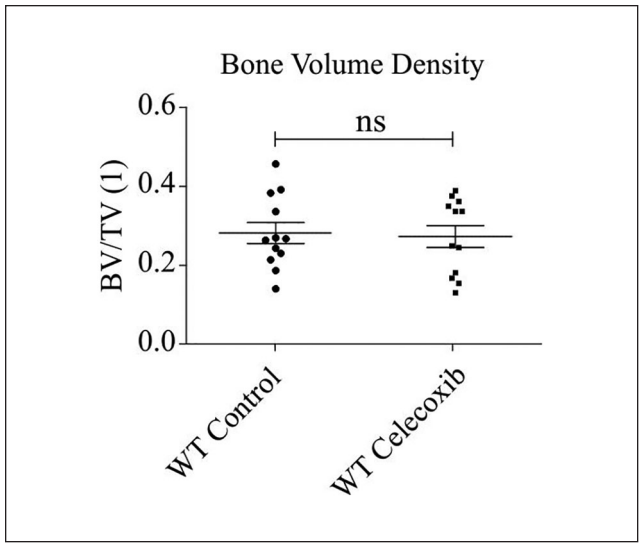

Figure 5. Bone microstructure analysis in growth plate area in control and celecoxib-treated mice. The bone microstructure was determined by micro–computed tomography (μCT). Quantification of bone volume density in volume of interest 3 (VOI-3) are determined. Each dot represents the determined value for each of the individual mice and lines in graphs indicate mean ± standard error of the mean (SEM). Statistical significance: $*P < 0.05$, ns = not significant.

the hypertrophic zone of the growth plate of COX-2 knockout and celecoxib-treated mice.

Currently, we cannot explain why decreased collagen type X expression and fewer and smaller hypertrophic chondrocytes do not result in a decreased thickness of the hypertrophic zone or skeletal consequences. Fewer and smaller cells in a similar cartilaginous volume suggest changes in extracellular matrix composition. Micro-CT scanning revealed a significantly increased bone volume fraction, bone density, and trabecular thickness in the mineralized tissue directly beneath the growth plate (**Fig. 3**) in the COX-2 treated animals compared to the placebo-treated animals. This observation is counterintuitive to the notion that COX-2 is involved in Runx2- and ALP-mediated ectopic bone formation[25] and osteoblast maturation[40] via BMP-2 and Wnt signaling, respectively. However, Xu *et al*.[41] postulated an important role for PTH/1,25-dihydroxy vitamin D_3 in bone volume density of COX-2 knockout mice. Although measured in already mature COX-2 knockout mice, these mice have increased bone volume fraction in the distal femur combined with increased serum parathyroid hormone and 1,25-dihydroxy vitamin D_3 levels, suggesting a hyperparathyroidism phenotype in these mice as a way to compensate for the loss of COX-2.[41] An increased bone (volume) density can also result from deregulated bone remodeling as COX-2-mediated PGE_2 expression is required for lipopolysaccharide-induced inflammatory bone resorption by osteoclasts[42] and pro-inflammatory M1 macrophage-enhanced osteogenesis of mesenchymal stem cells.[43] However, in this study, we did not detect significantly different numbers of TRAP-positive cells in the sub-growth plate region of celecoxib-treated (**Fig. 3**) or COX-2 KO mice (data not shown).

In this study, oral gavage with celecoxib started at 5 weeks of age when the mice were weaned. However, by then the majority of skeletal growth for these mice has already occurred.[44] More distinct differences in skeletal development would possibly become detectable when celecoxib treatment would start earlier, or when we would follow-up the animals longer than 15 weeks. Indeed, as shown in Supplemental Figure 5, at 5 weeks of age, the COX-2 KO mice did show more pronounced effects in a similar direction as at 15 weeks of age, especially for the tibia, regarding total growth plate thickness, thickness of the proliferative and hypertrophic zone, intensity of Safranin O staining, and bone length when compared with WT control littermates. On the other hand, from the age of 15 weeks, the growth plates in mice slowly start to prepare for the partial closure of the growth plate.[45] Considering that the celecoxib-treated mice show significantly higher glycosaminoglycan content in the growth plate combined, with lower collagen type X expression and higher bone density, it is a possibility that we are observing a premature closure of the growth plate in this group. Closure of the growth plate is difficult to measure in mice; however, Staines *et al*.[46] recently developed a new protocol for quantifying bony bridges the growth plate. Unfortunately, we could not test this protocol in our micro-CT data set. Nonetheless, we measured bone density in the noncalcified growth plate region (VOI-3). This revealed a higher bony density in this region in the celecoxib-treated mice, indicating premature growth plate closure (**Fig. 5**).

In summary, we could not detect differences in gross longitudinal growth of the murine proximal tibia or distal femur as a result of the genetic loss of COX-2 or inhibition of COX-2 enzyme activity by celecoxib. However, notable phenotypic features were observed in the maturation of the postnatal growth plate as a result of treatment with celecoxib, of which the potential consequences remain unclear at this point. Potential follow-up effects from the use of celecoxib on skeletal maturation of the long bones may warrant reevaluation of the use of celecoxib in skeletally developing individuals.

Authors' Note

This animal study and analysis was mainly performed at the Maastricht University Medical Center, except for the micro-CT analysis which was performed at the Eindhoven University of Technology.

Acknowledgments and Funding

The authors would like to thank the employees of the animal facility of the Maastricht University Medical Center (MUMC) for their assistance during this study and Dr. M. Poeze (Department of General Surgery, MUMC, the Netherlands) for providing the mice. The author(s) disclosed receipt of the following financial support for the research, authorship and/or publication of this article: The authors thank the Dutch Arthritis Association (Grant LLP14), the Dutch Stichting Annafonds | NOREF (Grant O2012/66) for their financial support.

Declaration of Conflicting Interests

The author(s) declared no potential conflicts of interest with respect to the research, authorship, and/or publication of this article.

Animal Welfare

All experiments were performed in accordance with relevant guidelines and regulations (ARRIVE, Animal Research: Reporting of In Vivo Experiments).

Ethical Approval

The experiment was approved by the Maastricht University animal ethical committee (MUMC DEC approval 2013-094).

Supplemental Material

Supplemental material for this article is available online.

ORCID iD

Marjolein M. J. Caron https://orcid.org/0000-0001-5316-9211

References

1. Kronenberg HM. Developmental regulation of the growth plate. Nature. 2003;423(6937):332-6.
2. Mackie EJ, Ahmed YA, Tatarczuch L, Chen KS, Mirams M. Endochondral ossification: how cartilage is converted into bone in the developing skeleton. Int J Biochem Cell Biol. 2008;40(1):46-62.
3. Park J, Gebhardt M, Golovchenko S, Perez-Branguli F, Hattori T, Hartmann C, *et al*. Dual pathways to endochondral osteoblasts: a novel chondrocyte-derived osteoprogenitor cell identified in hypertrophic cartilage. Biol Open. 2015;4(5):608-21.
4. Yang G, Zhu L, Hou N, Lan Y, Wu XM, Zhou B, *et al*. Osteogenic fate of hypertrophic chondrocytes. Cell Res. 2014;24(10):1266-9.
5. Zhou X, von der Mark K, Henry S, Norton W, Adams H, de Crombrugghe B. Chondrocytes transdifferentiate into osteoblasts in endochondral bone during development, postnatal growth and fracture healing in mice. PLoS Genet. 2014;10(12):e1004820.
6. Shim KS. Pubertal growth and epiphyseal fusion. Ann Pediatr Endocrinol Metab. 2015;20(1):8-12.
7. Chung R, Xian CJ. Recent research on the growth plate: mechanisms for growth plate injury repair and potential cell-based therapies for regeneration. J Mol Endocrinol. 2014;53(1):T45-T61.
8. Bonafe L, Cormier-Daire V, Hall C, Lachman R, Mortier G, Mundlos S, *et al*. Nosology and classification of genetic skeletal disorders: 2015 revision. Am J Med Genet A. 2015;167A(12):2869-92.
9. Superti-Furga A, Unger S. Nosology and classification of genetic skeletal disorders: 2006 revision. Am J Med Genet A. 2007;143(1):1-18.
10. Shroff R, Knott C, Gullett A, Wells D, Marks SD, Rees L. Vitamin D deficiency is associated with short stature and may influence blood pressure control in paediatric renal transplant recipients. Pediatr Nephrol. 2011;26(12):2227-3.
11. Zimmermann MB. The role of iodine in human growth and development. Semin Cell Dev Biol. 2011;22(6):645-52.
12. Gerstenfeld LC, Thiede M, Seibert K, Mielke C, Phippard D, Svagr B, *et al*. Differential inhibition of fracture healing by non-selective and cyclooxygenase-2 selective non-steroidal anti-inflammatory drugs. J Orthop Res. 2003;21(4):670-5.
13. Herbenick MA, Sprott D, Stills H, Lawless M. Effects of a cyclooxygenase 2 inhibitor on fracture healing in a rat model. Am J Orthop (Belle Mead NJ). 2008;37(7):E133-7.
14. Yoon DS, Yoo JH, Kim YH, Paik S, Han CD, Lee JW. The effects of COX-2 inhibitor during osteogenic differentiation of bone marrow-derived human mesenchymal stem cells. Stem Cells Dev. 2010;19(10):1523-33.
15. Zhang X, Schwarz EM, Young DA, Puzas JE, Rosier RN, O'Keefe RJ. Cyclooxygenase-2 regulates mesenchymal cell differentiation into the osteoblast lineage and is critically involved in bone repair. J Clin Invest. 2002;109(11):1405-15.
16. Welting TJ, Caron MM, Emans PJ, Janssen MP, Sanen K, Coolsen MM, *et al*. Inhibition of cyclooxygenase-2 impacts chondrocyte hypertrophic differentiation during endochondral ossification. Eur Cell Mater. 2011;22:420-36.
17. Dinchuk JE, Car BD, Focht RJ, Johnston JJ, Jaffee BD, Covington MB, *et al*. Renal abnormalities and an altered inflammatory response in mice lacking cyclooxygenase II. Nature. 1995;378(6555):406-9.
18. Brouwers JE, van Rietbergen B, Huiskes R. No effects of in vivo micro-CT radiation on structural parameters and bone marrow cells in proximal tibia of Wistar rats detected after eight weekly scans. J Orthop Res. 2007;25(10):1325-32.
19. Klinck RJ, Campbell GM, Boyd SK. Radiation effects on bone architecture in mice and rats resulting from in vivo micro-computed tomography scanning. Med Eng Phys. 2008;30(7):888-95.
20. Prockop DJ, Udenfriend S. A specific method for the analysis of hydroxyproline in tissues and urine. Anal Biochem. 1960;1:228-39.
21. Caron MM, Emans PJ, Sanen K, Surtel DA, Cremers A, Ophelders D, *et al*. The role of prostaglandins and COX-enzymes in chondrogenic differentiation of ATDC5 progenitor cells. PLoS One. 2016;11(4):e0153162.
22. Janssen MP, Caron MM, van Rietbergen B, Surtel DA, van Rhijn LW, Welting TJ, *et al*. Impairment of the chondrogenic phase of endochondral ossification in vivo by inhibition of cyclooxygenase-2. Eur Cell Mater. 2017;34:202-16.
23. Gu J, Lu Y, Li F, Qiao L, Wang Q, Li N, *et al*. Identification and characterization of the novel Col10a1 regulatory mecha-

nism during chondrocyte hypertrophic differentiation. Cell Death Dis. 2014;5:e1469.
24. Arikawa T, Omura K, Morita I. Regulation of bone morphogenetic protein-2 expression by endogenous prostaglandin E2 in human mesenchymal stem cells. J Cell Physiol. 2004;200(3):400-6.
25. Chikazu D, Li X, Kawaguchi H, Sakuma Y, Voznesensky OS, Adams DJ, *et al*. Bone morphogenetic protein 2 induces cyclo-oxygenase 2 in osteoblasts via a Cbfal binding site: role in effects of bone morphogenetic protein 2 in vitro and in vivo. J Bone Miner Res. 2002;17(8):1430-40.
26. Hellingman CA, Davidson EN, Koevoet W, Vitters EL, van den Berg WB, van Osch GJ, *et al*. Smad signaling determines chondrogenic differentiation of bone-marrow–derived mesenchymal stem cells: inhibition of Smad1/5/8P prevents terminal differentiation and calcification. Tissue Eng Part A. 2011;17:1157-67.
27. Javed A, Afzal F, Bae JS, Gutierrez S, Zaidi K, Pratap J, *et al*. Specific residues of RUNX2 are obligatory for formation of BMP2-induced RUNX2-SMAD complex to promote osteoblast differentiation. Cells Tissues Organs. 2009;189(1-4):133-7.
28. Steinert AF, Proffen B, Kunz M, Hendrich C, Ghivizzani SC, Nöth U, *et al*. Hypertrophy is induced during the in vitro chondrogenic differentiation of human mesenchymal stem cells by bone morphogenetic protein-2 and bone morphogenetic protein-4 gene transfer. Arthritis Res Ther. 2009;11(5):R148.
29. Hunziker EB. Mechanism of longitudinal bone growth and its regulation by growth plate chondrocytes. Microsc Res Tech. 1994;28(6):505-19.
30. Hunziker EB, Schenk RK, Cruz-Orive LM. Quantitation of chondrocyte performance in growth-plate cartilage during longitudinal bone growth. J Bone Joint Surg Am. 1987;69(2):162-73.
31. Carlevaro MF, Cermelli S, Cancedda R, Descalzi Cancedda F. Vascular endothelial growth factor (VEGF) in cartilage neovascularization and chondrocyte differentiation: auto-paracrine role during endochondral bone formation. J Cell Sci. 2000;113(Pt 1):59-69.
32. Gerber HP, Hillan KJ, Ryan AM, Kowalski J, Keller GA, Rangell L, *et al*. VEGF is required for growth and survival in neonatal mice. Development. 1999;126(6):1149-59.
33. Gerber HP, Vu TH, Ryan AM, Kowalski J, Werb Z, Ferrara N. VEGF couples hypertrophic cartilage remodeling, ossification and angiogenesis during endochondral bone formation. Nat Med. 1999;5(6):623-8.
34. Maes C, Stockmans I, Moermans K, Van Looveren R, Smets N, Carmeliet P, *et al*. Soluble VEGF isoforms are essential for establishing epiphyseal vascularization and regulating chondrocyte development and survival. J Clin Invest. 2004;113(2):188-99.
35. Wu G, Luo J, Rana JS, Laham R, Sellke FW, Li J. Involvement of COX-2 in VEGF-induced angiogenesis via P38 and JNK pathways in vascular endothelial cells. Cardiovasc Res. 2006;69(2):512-9.
36. Luo H, Chen Z, Jin H, Zhuang M, Wang T, Su C, *et al*. Cyclooxygenase-2 up-regulates vascular endothelial growth factor via a protein kinase C pathway in non-small cell lung cancer. J Exp Clin Cancer Res. 2011;30:6.
37. Hsu AL, Ching TT, Wang DS, Song X, Rangnekar VM, Chen CS. The cyclooxygenase-2 inhibitor celecoxib induces apoptosis by blocking Akt activation in human prostate cancer cells independently of Bcl-2. J Biol Chem. 2000;275(15):11397-403.
38. Chang JK, Wu SC, Wang GJ, Cho MH, Ho ML. Effects of non-steroidal anti-inflammatory drugs on cell proliferation and death in cultured epiphyseal-articular chondrocytes of fetal rats. Toxicology. 2006;228(2-3):111-23.
39. Li N, Wang Q, Zhu T, Qiao L, Zhang F, Mi R, *et al*. In vitro functional characterization of prostaglandin-endoperoxide synthase 2 during chondrocyte hypertrophic differentiation. Oncotarget. 2016;7(24):36280-92.
40. Nagano A, Arioka M, Takahashi-Yanaga F, Matsuzaki E, Sasaguri T. Celecoxib inhibits osteoblast maturation by suppressing the expression of Wnt target genes. J Pharmacol Sci. 2017;133(1):18-24.
41. Xu M, Choudhary S, Goltzman D, Ledgard F, Adams D, Gronowicz G, *et al*. Do cyclooxygenase-2 knockout mice have primary hyperparathyroidism? Endocrinology. 2005;146(4):1843-53.
42. Coon D, Gulati A, Cowan C, He J. The role of cyclooxygenase-2 (COX-2) in inflammatory bone resorption. J Endod. 2007;33(4):432-6.
43. Lu LY, Loi F, Nathan K, Lin TH, Pajarinen J, Gibon E, *et al*. Pro-inflammatory M1 macrophages promote osteogenesis by mesenchymal stem cells via the COX-2-prostaglandin E2 pathway. J Orthop Res. 2017;35:2378-85.
44. Somerville JM, Aspden RM, Armour KE, Armour KJ, Reid DM. Growth of C57BL/6 mice and the material and mechanical properties of cortical bone from the tibia. Calcif Tissue Int. 2004;74(5):469-75.
45. Kilborn SH, Trudel G, Uhthoff H. Review of growth plate closure compared with age at sexual maturity and lifespan in laboratory animals. Contemp Top Lab Anim Sci. 2002;41(5):21-26.
46. Staines KA, Madi K, Mirczuk SM, Parker S, Burleigh A, Poulet B, *et al*. Endochondral growth defect and deployment of transient chondrocyte behaviors underlie osteoarthritis onset in a natural murine model. Arthritis Rheumatol. 2016;68(4):880-91.